Dalton Transactions

Direct Synthesis of Functionalized PCN-333 via Linker Design for Fe^{3+} Detection in Aqueous Media

Journal:	*Dalton Transactions*
Manuscript ID	DT-ART-04-2018-001508.R1
Article Type:	Paper
Date Submitted by the Author:	18-May-2018
Complete List of Authors:	Zhang, Yingmu; Texas A&M University, Chemistry Yang, Xinyu; Texas A&M University, Chemistry Zhou, Hong-Cai; Texas A&M University, Chemistry

SCHOLARONE™
Manuscripts

Please do not adjust margins

Journal Name

ARTICLE

Direct Synthesis of Functionalized PCN-333 via Linker Design for Fe^{3+} Detection in Aqueous Media

Yingmu Zhang, Xinyu Yang, Hong-Cai Zhou*

Received 00th January 20xx,
Accepted 00th January 20xx

DOI: 10.1039/x0xx00000x

www.rsc.org/

A new luminescent mesoporous metal-organic framework (PCN-604) was successfully synthesized from trimetric clusters, $Al_3(O)(CH_3COO)_6$ and pyridine-based tritopic linkers, 4,4',4''-(pyridine-2,4,6-triyl)tribenzoicate (PTB) via a solvothermal reaction. The MOF with **MTN** topology possesses remarkable aqueous and thermal stability. Due to the efficient binding sites rendered by the pyridyl-based linkers, PCN-604 shows fast fluorescence response towards trace amount of Fe^{3+} ions in water in a fluorescence-quenching mode. The Stern-Volmer quenching constant is calculated to be 8.53 x 10^3 M^{-1} and the limit of detection is 6.2 μM, which convincingly demonstrate the capability of the MOF for Fe^{3+} detection.

Introduction

Metal-Organic Frameworks (MOFs), an emergent class of porous materials, have gathered intense attention in the past two decades. The judiciously selected metal clusters and organic linkers impart MOFs with unique properties, namely, intrinsic crystallinity, porosity, structural or functional diversity, and tunability, which make them promising candidates in many applications such as gas storage, separation, catalysis, drug delivery and sensing.[1-5] Among various MOFs, mesoporous MOFs with the ability to encapsulate large molecules like organometallic catalyst, nanoparticles and enzymes, have been extensively utilized in chemo/bio applications.[6, 7] However, in spite of the benefits brought by such encapsulation, the accommodation of functional large molecules sacrifices partial pore volume, which decreases the diffusion efficiency and accessibility of the subsequent-coming species. Hence, it would be ideal to directly synthesize mesoporous MOFs with functionalized building blocks, especially organic linkers.[8]

Iron is one of the most ubiquitous elements in life and environment. It plays indispensable role in many biological processes such as oxygen metabolism, electron transfer and synthesis of DNA and RNA.[9] Permissible limit of iron in drinking water given by the World Health Organization (WHO) is 0.3 mg/mL.[10] Both the deficiency and excess of Fe^{3+} from the normal permissible limit will break cellular homeostasis and cause serious biological disorders like microcytic hypochromic anemia and Alzheimer's disease.[11] To dates, many methods have been put forward for Fe^{3+} detection including liquid chromatography, inductively coupled plasma atomic mass spectrometry (ICP-MS) and atomic absorption spectrophotometry (AAS).[12-14] Among them, luminescent sensing stands out because of its portability, simplicity, fast and visible response. Accordingly, various luminescent materials have been designed and synthesized in the pursuit of sensing the metal ion with high sensitivity and selectivity.[15-18] Luminescent MOFs (LMOFs) with their unique photoluminescence properties have recently bloomed out as potential chemical sensors for Fe^{3+} recognition.[3, 19] However, most of luminescent MOFs exhibit moderate aqueous stability and rely on ion exchange mechanism for Fe^{3+} detection, which is time-consuming and sometimes leads to the collapse of MOF structures. Therefore, luminescent MOFs that display good aqueous stability as well as fast response towards Fe^{3+} ions in water system are pressingly needed.

MIL-100 series are promising candidates for Fe^{3+} detection due to their superb stability in water due to the inert bonds formed between the tritopic linkers and trimeric metal clusters.[20] The expanded version of MIL-100, known as PCN-333(M) (M= Fe, Al, Sc), can also survive such harsh conditions.[21, 22] Instead of large channels, PCN-333 contains large cavities with a diameter of 5.5 nm, which will not only prompt the pre-concentration of the analytes but also accelerate the diffusion of incoming species. However, the original PCN-333 shows no fluorescent response to Fe^{3+} ions due to the lack of efficient binding sites. Herein, in this work, through judicious selection of organic building blocks, we directly built a luminescent MOF of PCN-333, named as PCN-604, from aluminium trimetric clusters and pyridine-based 4,4',4'' -(pyridine-2,4,6-triyl)tribenzoic acid (H_3PTB) ligands. Like PCN-333, the MOF exhibits excellent thermal and chemical stability and the ultrapores can be activated directly through regular degas process for further usage. Working as a luminescent senor, PCN-604 shows intense luminescence in water and has promising sensitivity and selectivity towards trace amount of Fe^{3+} ions demonstrated by the high quenching constant of 2.85 x 10^4 M^{-1} and low detection limit of 6.2 μM.

Department of Chemistry, Texas A&M University, College Station, Texas 77840-3012, USA. E-mail: zhou@chem.tamu.edu

†Electronic Supplementary Information (ESI) available: [details of any supplementary information available should be included here]. See DOI: 10.1039/x0xx00000x

This journal is © The Royal Society of Chemistry 20xx

Please do not adjust margins

Experimental

Materials and Instrumentation

p-toluadehyde, 4-methylacetophenone, ammonium acetate, potassium permanganate ($KMnO_4$), aluminum chloride hexahydrate ($AlCl_3 \cdot 6H_2O$), N, N-diethylformamide (DEF), tetrafluoroacetic acid (TFA) were purchased from either VWR or Sigma Aldrich. Unless otherwise noted, all commercial chemicals were used without further purification. Synchrotron powder X-ray diffraction (PXRD) was carried out with Bruker D8-Discover diffractometer equipped with a Mo sealed tube (λ = 0.72768 Å) on the beamline 17-BM at the Advanced Photon Source, Argonne National Laboratory. In-house powder X-ray diffraction (PXRD) was carried out on a Bruker D8-Focus Bragg-Brentano X-ray powder diffractometer equipped with a Cu sealed tube (λ = 0.72768 Å) at 40 KV and 40 mA. UV-Vis spectra were recorded on Shimadzu UV-2450 spectrophotometer. Fluorescence spectra were collected on Horiba Fluorolog spectrofluorometer. Thermogravimetric analyses (TGA) were carried out on a Shimadzu TGA-50 thermal analyzer from temperature to 600 °C at a ramp rate of 5 °C /min in a flowing air atmosphere. Nuclear magnetic resonance (NMR) data were collected on a Mercury 300 spectrometer. Low pressure gas adsorption measurements were performed on an ASAP 2020 with the extra-pure quality gases.

Synthesis of H_3PTB

1,3-di-p-tolyl-propenone

In a 250 mL round-bottom flask, *p*-toluadehyde (6.0 g, 50 mmol), 4-methylacetophenone (6.8 g, 51 mmol) and 3 % aqueous sodium hydroxide (150 mL) were mixed and rigorously stirred at room temperature for 30 min. The mixture was then heated up to 60 °C and allowed to react for another 12 hours. After cooling to the room temperature, the resulted light-yellow precipitate was filtered, washed thoroughly with water and air-dried for next step without further purification.

2,4,6-tri-p-tolyl-pyridine

4-methylacetophenone (4.0 g, 30 mmol), 1,3-di-*p*-tolyl-propenone (7.0 g, 30 mmol) and sodium hydroxide (4.8 g, 120 mmol) were crashed together with pestle and mortar for about 2 hours until the mixture turned to yellow powder. The solid was then transferred into a round-bottom flask which contains an excess of ammonium acetate (20 g) dissolved in 200 mL ethanol. The reaction mixture was heated under reflux overnight. Upon cooling to the room temperature, the precipitate was filtered, washed with water three times and dried. The crude product was further purified by column chromatography (eluent: ethyl acetate : hexane = 10 : 1) to yield white solid (4.2 g, 40 %). ^{1}H NMR (300 MHz, $CDCl_3$): δ 8.07 (d, *J* = 8.3 Hz, 4H), 7.79 (s, 2H), 7.61 (d, *J* = 8.4 Hz, 2H), 7.28 (d, *J* = 8.4 Hz, 6H), 2.42, (s, 9H).

4,4',4'' -(pyridine-2,4,6-triyl)tribenzoic acid (H_3PTB)

In a 500 mL three-necked flask, 2,4,6-tri-p-tolyl-pyridine (1.62 g, 4.7 mmol) was added to a mixing solvent (pyridine/water=200 mL/50 mL). The reaction mixture was heated up to 100 °C and 32 g $KMnO_4$ was added in portions with 8 g each time. After 24 hours, the dark mixture was cooled down and filtered to give a clear filtrate. The organic solvent was vacuumed up and the aqueous phase was acidified with 6M hydrochloric acid (until pH < 3). The obtained pale-yellow solid was then filtered, washed with water and acetone several times and dried to give the pure product (1.89 g, 90%). ^{1}H NMR (300 MHz, dmso): δ 8.51 (d, *J* = 8.5 Hz, 4H), 8.44 (s, 2H), 8.25 (d, *J* = 8.5 Hz, 2H), 8.13 (d, *J* = 8.5 Hz, 6H).

Synthesis of PCN-604

In a 4 mL Pyrex vial, $AlCl_3 \cdot 6H_2O$ (30 mg, 124.2 mmol), H_3PTC (10mg, 22.8 mmol) and 270 μL TFA were ultrasonically dissolved in 2 mL N, N-diethylformamide (DEF). The mixture was then heated in a 135 °C oven for 2 days to afford white crystalline powder. Yield: 4 mg.

Activation of PCN-604

~ 50 mg as-synthesized PCN-604 samples were firstly washed with DMF (3 mL x 3) and acetone (3 mL x 3). The samples were again immersed in acetone to undergo solvent-exchange process with fresh acetone three times within 12 hours. Afterwards, the acetone was decanted and the mixture samples were dried under vacuum for 10 min, transferred into BET tube and then activated by the 'outgas' function of Micrometritics ASAP 2020 system for one hour at 150 °C before the gas sorption measurement by the instrument.

Fluorescence quenching and titration experiments

To study the sensing capability of PCN-604 towards metal ions, fifteen different metal ions, Na^+, K^+, Ag^+, Mg^{2+}, Ca^{2+}, Mn^{2+}, Fe^{2+}, Co^{2+}, Ni^{2+}, Cu^{2+}, Zn^{2+}, Cd^{2+}, Al^{3+}, Cr^{3+}, Fe^{3+} were chosen and tested. ~15 mg fully-grounded powder samples were soaked in 30 mL deionized water and ultrasonicately treated more than 30 min to prepare well-dispersed MOF suspension. Afterwards, 1 mL of 1mM aqueous solutions of the metal ions were added respectively to the 2 mL of as-prepared MOF suspension in cuvettes. In titration experiments, Fe^{3+} aqueous solution (1mM) was added to 2 mL of MOF suspension in an incremental manner from 50 μL to 1000 μL. All the corresponding fluorescence spectra were recorded at room temperature. The quenching percentage was calculated with the formula: $Q = (1 - I/I_0) \times 100\%$, where I_0 and I are the fluorescence intensity of the suspension before and after addition of analytes.

This journal is © The Royal Society of Chemistry 20xx

Results and discussion

In order to achieve the direct synthesis of functionalized PCN-333 structure, 4,4',4'' -(pyridine-2,4,6-triyl)tribenzoic acid (H_3PTB) was chosen and synthesized with a modified procedure based on previously reported literature (Scheme S1).[23] Unlike other tritopic linkers functionalized with hanging substituents such as 1,3,5-benzentribenzoic acid (H_3BTB) and its derivatives, the pyridine-based linker is only decorated with one nitrogen atom on the central benzene, which not only serves as an additional binding site, but also, more importantly, releases the rotating steric hindrance when building MOFs, allowing the six oxygen atoms on the linker to stay in the same plane to adopt approximate D_{3h} symmetry, an indispensable prerequisite of forming **MTN** topology.[22, 24] The synthesis of PCN-604 was guided by the kinetically tuned dimensional augmentation (KTDA) method with $AlCl_3$ and H_3PTB as starting materials.[25] As confirmed by the powder X-ray diffraction (PXRD) patterns, PCN-604 is isostructural to PCN-333 and shares the same cubic **MTN** topology (Fig. S1).[21] The corresponding structural model of PCN-604 was simulated based on the reported PCN-333 structure by Material Studio 6.0.[26] The space group, $Fd\bar{3}m$, was used to describe the MOF structure. PCN-604 is composed of hybrid supertetrahedra building units connected in a vertex sharing manner, leading to a mesoporous structure. The supertetrahedra consist of aluminum octahedral trimers at the four vertexes linked by the organic linkers occupied at the four faces. Like PCN-333, PCN-604 also exhibits two types of mesoporous cages. The smaller cage is built of 20 supertetrahedra sharing vertex with a pentagonal window of 25.9Å in diameter. The larger cage is hexacaidecahedral (hexagonal-truncated trapezohedral) formed by 24 supertetrahedra, displaying both pentagonal windows and hexagonal windows of 30 Å in diameter. The large cage lies in a honeycomb arrangement in the [111] projection. The inner diameter is 11 Å for the super tetrahedral cage, 34 Å for the dodecahedral cage and 55Å for the hexacaidecahedral cage.

Porosity and stability characterization

As PTB shares almost the same size with 4,4',4''-s-triazine-2,4,6-triyl-tribenzoic acid (TATB), the porosity of PCN-604 is close to that of PCN-333(Al). Instead of activation with supercritical CO_2, which is usually used to degas mesoporous MOFs, the as-synthesized PCN-604 can be activated in common way.[21, 27] N_2 adsorption was performed at 77 K to determine the porosity of PCN-604. The MOF shows 1952 cm^3/g (STP) total N_2 uptake. The Brunauer–Emmett–Teller surface area and Langmuir surface area are 2633 m^2/g and 3561 m^2/g respectively. Two steep increases at P/P_0 = 0.35 and 0.5 on the N_2 adsorption isotherm correspond to the two types of mesoporous cages. The experimental pore volume is 3.2 cm^3/g, slightly less than that of PCN-333 (3.85 cm^3/g) (Table S1). Aqueous stability tests are also performed via water treatment. The as-activated samples are immersed into aqueous solutions with various pH values and are allowed to stay overnight. PXRD patterns indicate that PCN-604 can survive in pure water and aqueous solutions with pH from 3 to 8 (Fig. 1a). The N_2 isotherms are also tested after water treatment. According to the N_2 isotherm, the crystallinity of PCN-604 slightly decreased after acid or base treatment, as the N_2 uptake reduced to 1698 cm^3/g (Fig. 1b). Thermal stability of PCN-604 is determined by thermogravimetric analysis (TGA) (Fig. S4). It shows that the decomposition temperature of PCN-604 is 540 °C and the three weight losses are corresponded to

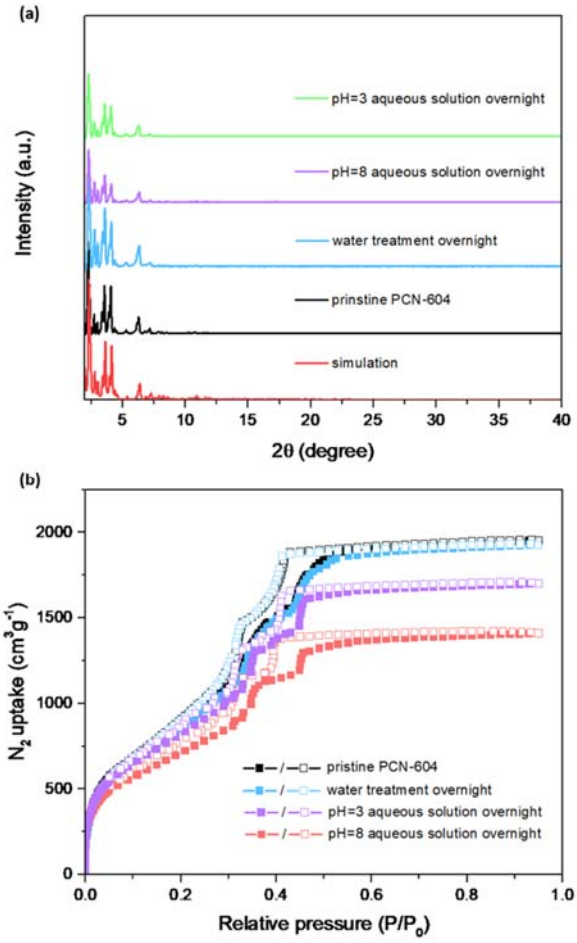

Fig. 1. (a) PXRD patterns of simulation PCN-604 (red), pristine PCN-604 (black), samples treated with water, pH = 8 aqueous solution (purple) and pH = 3 aqueous solution (green). (a) N_2 sorption isotherms of pristine PCN-604 (black), samples treated with water (blue), pH = 3 aqueous solution (purple) and pH = 8 aqueous solution (red-pink) at 77k.

the departure of free solvent (up to 100 °C), coordinated solvent (230 °C) and combustion of the organic ligand (490 °C). The desired aqueous stability as well as the excellent thermal stability can be ascribed to the strong electrostatic interaction between the trivalent aluminium clusters and carboxylate linkers.

Luminescence properties

Considering that PCN-604 is built of Al^{3+} metal clusters with complete electron subshells and electron-rich π-conjugated ligands, the obtained network is supposed to be photoactive for further applications.[15] The photoluminescence properties of both PCN-604 and its acid ligand H_3PTB in solid state were firstly

explored at room temperature. According to the solid-state fluorescence spectra, the free acid ligand shows strong emission centered at 475 nm and 640 nm when excited at 424 nm, assigned to π → π* and n → π* transitions respectively (Fig.S10); while PCN-604 cannot be fully excited at the same excitation wavelength, even though it displays similar emission profile compared to its acid ligand (Fig.S8). PCN-604 exhibits intense fluorescence emission upon 382 nm excitation with the maximum emission peak at 433 nm (Fig.S9). The notable difference in fluorescence properties might be induced by ligand-to-metal charge transfer (LMCT) in the coordination material.[28] The fluorescence properties of PCN-604 dispersed in different solvents are also investigated (Fig.S11). The fluorescence spectra indicate trivial solvent effect of the MOF suspension in most organic solvents like acetone, DMF, THF, CH_3CN, MeOH, EtOH, CH_2Cl_2 displaying maximum emission peaks centred at 379 nm upon excitation of 350 nm. It should be pointed out that, compared with the spectra of other solvents, there is an additional shoulder peak at 423 nm in weak-polar solvent CH_2Cl_2, which might be caused by the pyridyl group.[29] [30] The shoulder emission disappears with the increasing of solvent polarity. When it comes to water, a broader emission occurs with a blue-shift of 10nm, demonstrating the existence of the hydrogen bond interactions between the H_2O molecules and organic ligands.[31, 32] Fluorescence lifetime of the MOF suspension was also measured, showing a multi-exponential decay. The amplitude-weighted average lifetime (τ_{av}) is calculated to be 5.33 ns (Fig.S12-13).

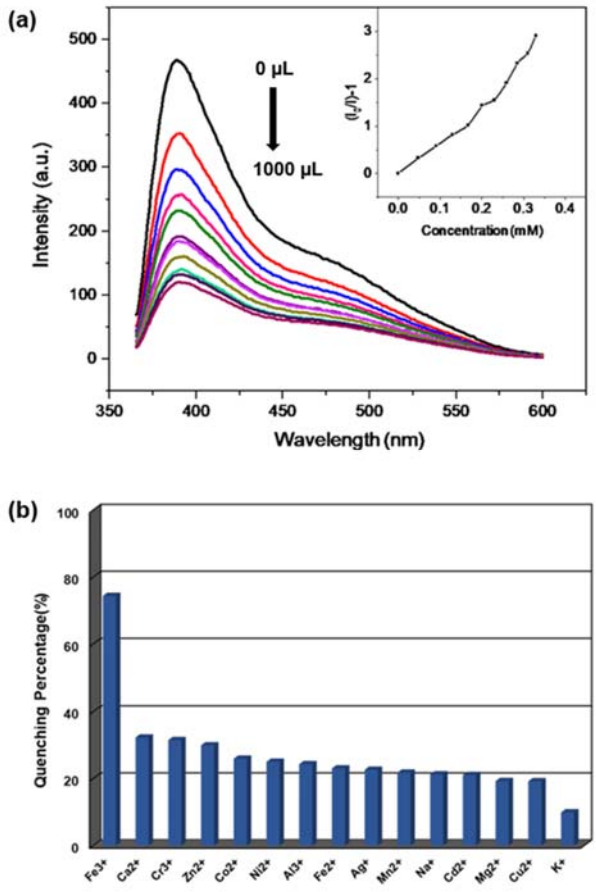

Fig. 2. (a) Fluorescence spectra of PCN-604 suspension in response to different concentrations of Fe^{3+}. Fe^{3+} aqueous solution (1 mM) was added gradually from 0 μL to 1000 μL (100 μL each time). (b) Fluorescence quenching of PCN-604 dispersed in aqueous solutions of fifteen different metal cations (1 mM). Excitation at 350 nm, room temperature.

Sensing measurements

Considering the desired chemical stability, fluorescence performance as well as the efficient pyridyl binding site of PCN-604, we investigated the sensing capability of the as-synthesized MOF towards various metal ions in water. 2 mg/mL aqueous suspensions of MOF powder were ultrasonicately prepared and 1 mM aqueous solutions of fifteen different nitrate salts of metal cations, Na^+, K^+, Ag^+, Mg^{2+}, Ca^{2+}, Mn^{2+}, Fe^{2+}, Co^{2+}, Ni^{2+}, Cu^{2+}, Zn^{2+}, Cd^{2+}, Al^{3+}, Cr^{3+}, Fe^{3+}, were added to the suspensions respectively. Fluorescence intensities of these suspensions before and after the additions of metal ions were all recorded at room temperature upon excitation at 350 nm and the quenching efficiencies were calculated and compared for qualitative studies of sensitivity. According to the fluorescence spectra, these metal ions exert different quenching effects on the fluorescence of PCN-604. Among them, Fe^{3+} causes the highest fluorescence quenching in respect of emission intensities with the quenching efficiency of 74%; while others display either moderate or negligible quenching efficiencies (from 10% to 30%) as shown in Fig.2b. It is also worthy to note that the fluorescence quenching occurs within 1 min, a rapid response which might be due to intrinsic mesoporous structure of PCN-604 that allows the analyte to diffuse and interact the host network rapidly. The selectivity of PCN-604 for Fe^{3+} detection was also explored based on competitive experiments in the coexistence of other metal ions. 1 mL aqueous solution that contains various metal ions except for Fe^{3+} (1 mM for each) was introduced to 1 mL MOF suspension, leading to a decrease in fluorescence intensity by 18.6 %. The change is similar to that caused by the individual addition of these metal ions, indicating no accumulative quenching effects. Sequential addition of 1 mL aqueous solution of Fe^{3+} (1mM) to the suspension resulted in a dramatic fluorescent quenching by 64 %, which demonstrates that the sensing process is resistant to the interference of other metals. As a control experiment, the fluorescent intensities of the mixture of MOF suspension and deionized water were also tested and the presence of deionized water slightly lowered the intensity by 17.4 % due to the dilution of the original suspension (Fig.S16).

To further validate the high sensitivity for Fe^{3+} detection, titration experiments were carried out with the concentration of Fe^{3+} ranging from 0 to 1000 μM. With the gradual addition of Fe^{3+} ion, the fluorescence intensity of the suspension was steadily quenched to the lowest point. The quenching constant (K_{sv}) was further calculated based on the Sterm-Volmer (SV)

This journal is © The Royal Society of Chemistry 20xx

equation: $(I_0/I) = 1 + K_{sv}[M]$, where I_0 is the initial intensity, I is the intensities of the corresponding MOF suspensions varying with different concentrations of Fe^{3+} ([M]), and K_{sv} is the quenching constant (M^{-1}), which is an important indicator of sensing ability of a fluorescent sensor.[29] It is shown that the SV-plot presents quiet a linear shape in the low concentration range and slightly upper bends at high concentration level (Fig.2a). k_{sv} value is calculated to be 8.53×10^3 M^{-1} based on the linear part and which is better, if not, comparable to previously reported MOF-based Fe^{3+} sensors (Table S2). The limit of detection (LOD) turns to be 6.2 μM calculated from the K_{sv} value and standard deviation S_b of three repeated fluorescence measurements of blank solutions ($3S_b/K_{sv}$). The large K_{sv} value and small LOD demonstrate the great feasibility of PCN-604 to serve as a fluorescent sensor for Fe^{3+} detection in aqueous system.

Mechanism

Several possible mechanisms have been well documented to explain the fluorescence quenching by Fe^{3+} ions including the collapse of the framework structure, ion exchange, host-and-guest interactions via fluorescence resonance energy transfer (FRET) or/ and photoinduced electron transfer (PET).[33-35] The maintained crystallinity of PCN-604 after Fe^{3+} treatment is demonstrated by the PXRD patterns, which excludes the possibility of structural collapse. In addition, the rapid quenching effect (with several seconds) and the strong covalent bonds formed between the high valent Al^{3+} clusters and carboxylate groups can, to some extent, rule out the ion exchange between the externally induced Fe^{3+} and the framework, which is time-consumed and kinetic-driven. Hence, one can propose that the main mechanism for the fluorescence quenching effect is the host-guest interaction. With the unsaturated 3d orbital ($3d^5$ $4s^0$), the highly charged Fe^{3+} is a better electron acceptor compared to other cations; meanwhile, the organic linkers with conjugated moieties turn out to be good electron donors. Herein, the quenching effect is likely to originate from the photoinduced electron transfer(PET). Upon excitation, the excited electrons are proposed to be transferred to the lowest unoccupied molecular orbital (LUMO) of Fe^{3+}. The process leads to nonradiative pathway and is competitive to radiative LMTC within the framework, impeding the fluorescence of the MOF. Moreover, the N atoms on the pyridine groups of the organic linkers can donate their lone-pair electrons to the metal ion, enhancing the interactions between the targeted analytes and the host material. As a result, the fluorescence quenching is triggered. It is also reasonable that the sensing mechanism underlies the distance-dependent fluorescence resonance energy transfer (FRET). In order to prove it, the adsorption spectra of various metal ions were collected. The absorption of Fe^{3+} has the largest degree of overlapping with the emission of PCN-604, making the energy transfer feasible. The overlap for other metal ions is negligible and is in good agreement with the trend of quenching efficiency (Fig.S17).

Conclusions

To conclude, we successfully synthesized a novel mesoporous MOF (PCN-604) from predesigned functional organic linkers through direct synthesis method. PCN-604 is constructed from trimetric aluminium clusters and 4,4',4''-(pyridine-2,4,6-triyl)tribenzoic acid (H_3PTB). The crystallinity and porosity of the MOF are confirmed by the powder X-ray diffraction combined with N_2 isotherms. The stability of PCN-604 is evaluated through water treatments and thermogravimetric analysis (TGA), showing that the material can sustain its crystallinity in the aqueous solutions with pH in the range of 3-8 and will not decompose below 540 °C. Fluorescence properties of the MOF in both solid state and solutions are explored based on the excitation and emission spectra as well as fluorescent lifetime showing the material displays good emission in water. Notably, the fluorescence of PCN-604 can be quenched rapidly within seconds by the aqueous solution of Fe^{3+}. The rapid quenching process can be ascribed to the mesoporous cavities of the network that can pre-concentrate the analytes and hinder the diffusion constrains. The quenching efficiency of Fe^{3+} is 74%, the highest one compared to those of other metal cations. Moreover, verified by the quenching testes and titration experiments, PCN-604 possesses satisfactory sensitivity and selectivity indicated by the large quenching constant and detection limit, 8.53×10^3 M^{-1} and 6.2 μM, respectively. To have a deep look, the good sensing performance is driven by the host-guest interactions involving fluorescence resonance energy transfer (FRET) or/ and photoinduced electron transfer (PET) and the intrinsic electron-donating pyridine groups on the linker also plays an essential rule during the sensing process.

Conflicts of Interest

There are no conflicts of interest to declare.

Acknowledgements

This work was supported by the Center for Gas Separations Relevant to Clean Energy Technologies, an Energy Frontier Research Center funded by the U.S. Department of Energy, Office of Science, Office of Basic Energy Sciences (DE-SC0001015), U.S. Department of Energy, Office of Fossil Energy, National Energy Technology Laboratory (DE-FE0026472), and Robert A. Welch Foundation through a Welch Endowed Chair to HJZ (A-0030).

Notes and references

1. K. Sumida, D. L. Rogow, J. A. Mason, T. M. McDonald, E. D. Bloch, Z. R. Herm, T.-H. Bae and J. R. Long, *Chem. Rev.*, 2011, **112**, 724-781.
2. X. Lian, Y. Fang, E. Joseph, Q. Wang, J. Li, S. Banerjee, C. Lollar, X. Wang and H.-C. Zhou, *Chem. Soc. Rev.*, 2017, **46**, 3386-3401.

3. Z. Hu, B. J. Deibert and J. Li, *Chem. Soc. Rev.*, 2014, **43**, 5815-5840.
4. J.-R. Li, J. Sculley and H.-C. Zhou, *Chem. Rev.*, 2011, **112**, 869-932.
5. M. Yoon, R. Srirambalaji and K. Kim, *Chem. Rev.*, 2011, **112**, 1196-1231.
6. W. Xuan, C. Zhu, Y. Liu and Y. Cui, *Chem. Soc. Rev.*, 2012, **41**, 1677-1695.
7. X. Lian, Y.-P. Chen, T.-F. Liu and H.-C. Zhou, *Chem. Sci.*, 2016, **7**, 6969-6973.
8. W. Lu, Z. Wei, Z.-Y. Gu, T.-F. Liu, J. Park, J. Park, J. Tian, M. Zhang, Q. Zhang and T. Gentle III, *Chem. Soc. Rev.*, 2014, **43**, 5561-5593.
9. S. R. Lynch, *Nutr. Rev.*, 1997, **55**, 102-110.
10. W. H. Organization, *Guidelines for drinking-water quality: recommendations*, World Health Organization, 2004.
11. N. C. Andrews, *N. Engl. J. Med.*, 1999, **341**, 1986-1995.
12. F. Séby, S. Charles, M. Gagean, H. Garraud and O. Donard, *J. Anal. At. Spectrom.*, 2003, **18**, 1386-1390.
13. D. Yuan, D. Fu, R. Wang and J. Yuan, *Spectrochim. Acta. Part A*, 2008, **71**, 276-279.
14. Z. Sun and P. Liang, *Microchimica Acta*, 2008, **162**, 121-125.
15. Y. Zhang, S. Yuan, G. Day, X. Wang, X. Yang and H.-C. Zhou, *Coord. Chem. Rev.*, 2018, **354**, 28-45.
16. W. Gao, F. Liu, B.-Y. Zhang, X.-M. Zhang, J.-P. Liu, E.-Q. Gao and Q.-Y. Gao, *Dalton Trans.*, 2017, **46**, 13878-13887.
17. X. Dao and Y. Ni, *Dalton Trans.*, 2017, **46**, 5373-5383.
18. Z. Qian, J. Ma, X. Shan, H. Feng, L. Shao and J. Chen, *Chem. Eur. J.*, 2014, **20**, 2254-2263.
19. W. P. Lustig, S. Mukherjee, N. D. Rudd, A. V. Desai, J. Li and S. K. Ghosh, *Chem. Soc. Rev.*, 2017, **46**, 3242-3285.
20. G. Férey, C. Mellot-Draznieks, C. Serre, F. Millange, J. Dutour, S. Surblé and I. Margiolaki, *Science*, 2005, **309**, 2040-2042.
21. D. Feng, T. F. Liu, J. Su, M. Bosch, Z. Wei, W. Wan, D. Yuan, Y. P. Chen, X. Wang, K. Wang, X. Lian, Z. Y. Gu, J. Park, X. Zou and H. C. Zhou, *Nat Commun*, 2015, **6**, 5979.
22. P. Horcajada, H. Chevreau, D. Heurtaux, F. Benyettou, F. Salles, T. Devic, A. Garcia-Marquez, C. Yu, H. Lavrard, C. L. Dutson, E. Magnier, G. Maurin, E. Elkaim and C. Serre, *Chem Commun (Camb)*, 2014, **50**, 6872-6874.
23. Q. Yao, A. Bermejo Gómez, J. Su, V. Pascanu, Y. Yun, H. Zheng, H. Chen, L. Liu, H. N. Abdelhamid, B. Martín-Matute and X. Zou, *Chem. Mater.*, 2015, **27**, 5332-5339.
24. J. Park, D. Feng and H. C. Zhou, *J. Am. Chem. Soc.*, 2015, **137**, 1663-1672.
25. D. Feng, K. Wang, Z. Wei, Y.-P. Chen, C. M. Simon, R. K. Arvapally, R. L. Martin, M. Bosch, T.-F. Liu and S. Fordham, *Nat Commun*, 2014, **5**, 5723.
26. I. Accelrys, *Accelrys Software Inc*, 2010.
27. D. Feng, K. Wang, J. Su, T. F. Liu, J. Park, Z. Wei, M. Bosch, A. Yakovenko, X. Zou and H. C. Zhou, *Angew. Chem. Int. Ed. Engl.*, 2015, **54**, 149-154.
28. C. X. Yang, H. B. Ren and X. P. Yan, *Anal. Chem.*, 2013, **85**, 7441-7446.
29. B. Wang, Q. Yang, C. Guo, Y. Sun, L. H. Xie and J. R. Li, *ACS Appl Mater Interfaces*, 2017, **9**, 10286-10295.
30. Y. Zhang, C. B. Murphy and W. E. Jones, *Macromolecules*, 2002, **35**, 630-636.
31. X. Luo, X. Zhang, Y. Duan, X. Wang and J. Zhao, *Dalton Trans.*, 2017, **46**, 6303-6311.
32. S. Mostakim and S. Biswas, *CrystEngComm*, 2016, **18**, 3104-3113.
33. J. C. Jin, L. Y. Pang, G. P. Yang, L. Hou and Y. Y. Wang, *Dalton Trans.*, 2015, **44**, 17222-17228.
34. H. Li, Y. He, Q. Li, S. Li, Z. Yi, Z. Xu and Y. Wang, *RSC Adv.*, 2017, **7**, 50035-50039.
35. R. Lv, Z. Chen, X. Fu, B. Yang, H. Li, J. Su, W. Gu and X. Liu, *J. Solid State Chem.*, 2018, **259**, 67-72.

This journal is © The Royal Society of Chemistry 20xx